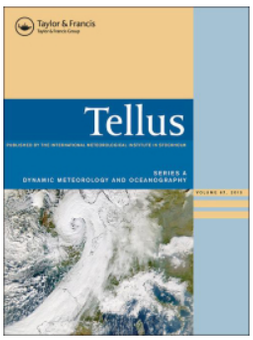

Tellus A: Dynamic Meteorology and Oceanography

ISSN: (Print) (Online) Journal homepage: https://www.tandfonline.com/loi/zela20

Impact of strong and extreme El Niños on European hydroclimate

Martin P. King, Entao Yu & Jana Sillmann

To cite this article: Martin P. King, Entao Yu & Jana Sillmann (2020) Impact of strong and extreme El Niños on European hydroclimate, Tellus A: Dynamic Meteorology and Oceanography, 72:1, 1-10, DOI: 10.1080/16000870.2019.1704342

To link to this article: https://doi.org/10.1080/16000870.2019.1704342

Tellus SERIES A DYANAMIC METEOROLOGY AND OCEANOGRAPHY
PUBLISHED BY THE INTERNATIONAL METEOROLOGICAL INSTITUTE IN STOCKHOLM

Impact of strong and extreme El Niños on European hydroclimate

By MARTIN P. KING[1]*, ENTAO YU[2], and JANA SILLMANN[3], [1]*NORCE Norwegian Research Centre, Bjerknes Centre for Climate Research, Bergen, Norway;* [2]*Nansen-Zhu International Research Centre, Institute of Atmospheric Physics, Chinese Academy of Sciences, Beijing, China;* [3]*Center for International Climate and Environmental Research Oslo (CICERO), Oslo, Norway*

(Manuscript Received 30 August 2019; in final form 5 December 2019)

ABSTRACT

The question of European hydroclimate anomaly associated with El Niño-Southern Oscillation (ENSO) is revisited by composite analyses on data from Dai et al.'s Palmer Drought Severity Index, the Old World Drought Atlas (OWDA), and a 10-member CESM coupled-model Last Millennium Ensemble (CESM-LME) simulations. This study benefits from exceptionally long or large samples in OWDA and CESM-LME. The averagely strong El Niño (1–2 standard deviations, or about one event per decade) is correlated to wet condition in western and southern Europe, and dry condition in Northern Europe; this result agrees with previous studies and thus provides a further support to this scenario. We also find in OWDA that extremely strong El Niño (>2 standard deviation, or about one event every 70–100 years) is related to a dry condition in western Europe. This suggests that the extreme El Niño impact in western Europe is opposite, or at least not linear, to that for the averagely strong El Niño. The impact of extreme El Niño does not appear to be reproduced by the LME, and will require further analyses on other climate reconstructions and models data.

Keywords: ENSO teleconnection, European hydroclimate, impacts of extreme El Nino

1. Introduction

El Niño-Southern Oscillation (ENSO) is a strong climate driver in the interannual timescales, its climate impact is wide-ranging in the Asia-Pacific region. However, its impact further afield such as over the North Atlantic–Europe (NAE) sector is more challenging to establish (van Oldenborgh and Burgers, 2005; Deser et al., 2017), remains debated and is a topic of ongoing research. This is despite previous studies which argue for robust climate impact over Europe (e.g. Brönnimann et al., 2007; Brönnimann, 2007). Brönnimann et al. (2007) analysed various early instrumental data, reconstructed fields and times series for the past 500 years. Their findings (e.g. see their Fig. 8) show that El Niño is connected to cold anomaly in northern Europe, and to warm anomaly in southern Europe and Turkey during winter (January–March). While for precipitation, El Niño is connected to negative anomaly in Scandinavia and positive anomaly in southern Europe. The presented relationships for La Niña events are symmetrical to those for El Niños. These ENSO climate impacts in Europe overall have a north–south contrast. Furthermore, they are also consistent with the teleconnection of ENSO in the NAE through the North Atlantic Oscillation (NAO), such that negative (positive) NAO is connected to El Niño (La Niña) (e.g. King et al., 2018a and references therein).

In this short article, we present results of investigating the ENSO and NAE hydroclimate relationships mainly using two datasets which were made available relatively recently (the Old World Drought Atlas and the CESM Last Millennium Ensemble, to be described in the next section). These long datasets ameliorate the problem of obtaining statistical significant signal; and they also allow the most extreme ENSO events to be studied statistically which is otherwise not possible because there are too few of these events during the instrumental period. We focus on the aforementioned relationship in these datasets and how well they agree with previous findings, on how the simulated relationships are compared to other data and on what the effects of the most extreme ENSO events are.

Researchers have reported increased occurrence of ENSO events under future greenhouse warming (e.g. Cai et al., 2014, 2015), a result which has an implication for

*Corresponding author. e-mail: martin.king@norceresearch.no

Citation: Tellus A: 2020, **72**, 1704342, https://doi.org/10.1080/16000870.2019.1704342

future climate impacts of ENSO. ENSO is also an important physical source of seasonal climate predictability in NAE (e.g. Scaife et al., 2014, 2017; King et al., 2018a). These factors together with ENSO's potential climate impacts in NAE mean that the current research also has a practical relevance.

2. Data and methods

The Old World Drought Atlas (OWDA, Cook et al., 2015) is formulated in year-by-year reconstructed summer (JJA, growing season in the Northern Hemisphere) Palmer Drought Severity Index (PDSI) on a half-a-degree grid for Europe and available for the last two millennia. It was created using tree-ring chronologies from living and subfossil trees, as well as from archaeological and historical tree-ring data. The OWDA is indicative of soil moisture condition in the spring and summer seasons (Cook et al., 2015) because droughts or pluvials conditions can be resulted from cumulative rather than purely instantaneous effects.

The Community Earth System Model-Last Millennium Ensemble (LME) is an ensemble of the global earth system model (CESM v. 1.1) experiments ran under a full set of transient past climate forcings (solar variability, orbital changes, volcanic eruptions, land use/cover, greenhouse gases, ozone/aerosols) for 850 CE to 2005 CE (for further details, see Otto-Bliesner et al., 2016). We use data from 10 members that were available at the start of this study. Otto-Bliesner et al. (2016) present the simulated climate periods and trends in the last millennium, including those found in the anthropogenic warming era. In Yu et al. (2018), we examined the SST simulated in the LME. It was found that, compared to observation, the model produced higher amplitudes of SST variability over wider ocean areas. Its ENSO-related SST anomaly also occurs over all ocean basins including the Atlantic Ocean, compared to observation where it is mainly confined to certain parts of the Pacific and Indian Oceans (Figs. 3, 8, S1 in Yu et al., 2018). This factor may have contributed to the homogeneous PDSI anomalies related to ENSO over more extended areas in Asia produced by the LME when compared to observational PDSI where the statistical significant anomalies are more limited in areas (Yu et al., 2018). We will discuss this aspect for NAE in Section 3.

To calculate the PDSI values in LME, first we estimate potential evapotranspiration (PET) based on the equation of Thornthwaite (1948) which requires near-surface air temperature as an input. Next, using PET and precipitation, the Thornthwaite water balance and the so-called Palmer moisture anomaly index (Z index) are obtained; the PDSI is then a time evolution of Z index and preceding PDSI values (for more details and references, see Wells et al., 2004; Yu et al., 2018). As in Yu et al. (2018), we follow the PDSI calculation algorithm of Jacobi et al. (2013) but here adapted to the NCAR Command Language (NCL) to apply on gridded data such as the LME in the current research. Examining the PDSI values in LME for Asia (Fig. S1 in Yu et al., 2018) and Europe (not shown) indicates that the model PDSI variability (standard deviation) can be up to a *maximum* of 20% weaker than observation (i.e. within instrumental period) in some parts of western Europe. But the overall PDSI variation in space is captured by the model; further comparisons are done in Section 3.

PDSI has some limitations such as it assumes all precipitation is immediately available in the water balance and thus is most valid for the low-to-mid latitudes locations where delayed water availability due to snow and ice melt is non-existent or limited. Despite the limitations, Dai et al. (2004), Dai (2011) showed that PDSI values correlate significantly with measured soil moisture during the warm seasons. Adopting the PDSI in the current study is also needed as OWDA is formulated in this index; the comparisons and analyses in this study are made consistently with PDSI. A further limitation is that there is no universal interpretation of what drought is, there are many existing definitions, and there was no standard procedure that allows the different definitions to be compared consistently. Raible et al. (2017) proposed a standard and flexible template of calculations that allows different drought definitions to be calculated so that they can be assessed together in their true reflections of droughts. Such extensive analyses and inter-comparisons of different drought indices is beyond the resources of our current study; but we note that PDSI is already a more sophisticated/complex drought index compared to the others.

Our analysis mainly uses the standard composite method where the average of selected anomalous events (e.g. in PDSI) is calculated. The events could be selected based on a reference variable that is related to El Niño or La Niña (e.g. Niño3.4) at values exceeding a threshold. The Niño3.4 time series used in the analysis of the model data is the standard one defined as the average monthly sea surface temperature anomaly in the area 170°W–120°W, 5°S–5°N. ENSO normally develops and decays over a period of less than a year. However, PDSI is designed to track cumulative effects in wet or dry spells and may not be able to indicate variations in shorter timescales such as from season to season. The PDSI calculated has a e-folding time of about 6 months (Raible et al., 2017). One important assumption of our study is that strong and extreme ENSO events can provide a "shock" to the surface water balance so that we can

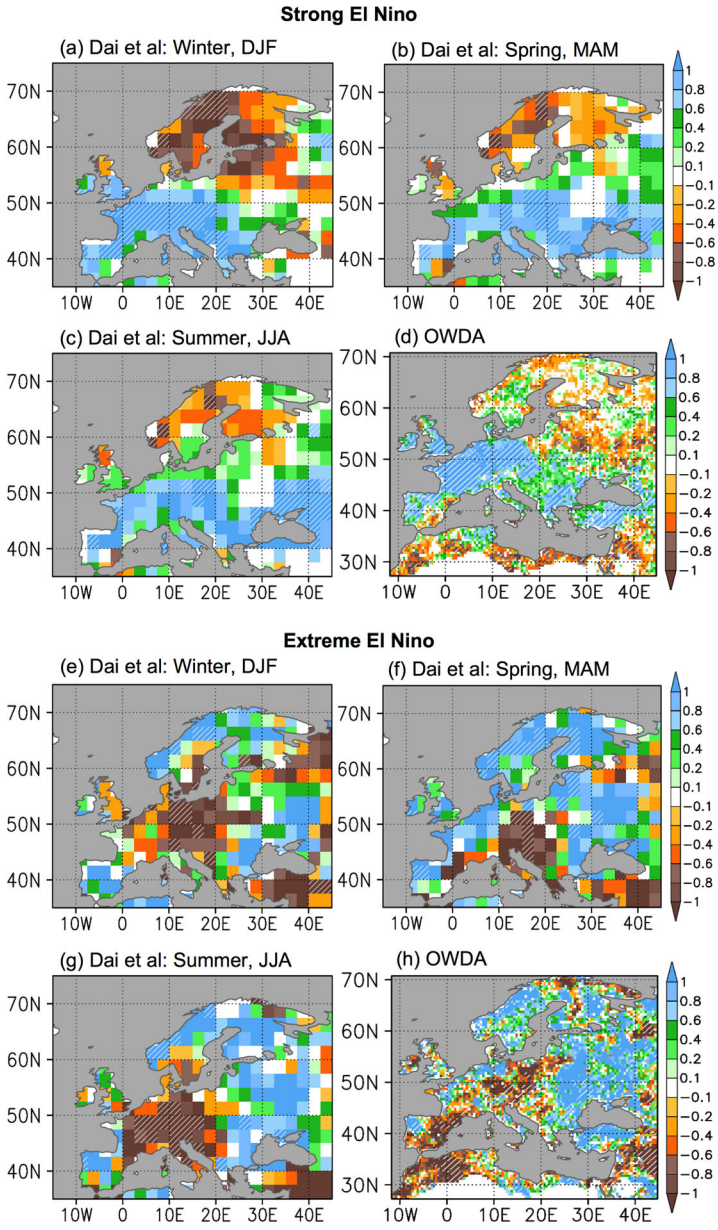

Fig. 1. Panels a, b, c are PDSI composites for strong El Ninos (15 events from Dai et al's PDSI for 1900–2014 C.E) for the seasons indicated; panel d is OWDA's PDSI composite for exactly the same events. Panels e, f, g are PDSI composites for extreme El Ninos (three events: 1972/73, 1982/83, 1997/98); panel h is OWDA's PDSI composite for exactly the same events. El Nino events selected are the same as Brönnimann et al. (2007) for the instrumental period and excluding events following volcanic eruptions or extreme El Ninos. Grid points with at least 95% statistical significance are indicated with white colour hatching.

detect the effects in PDSI over the warmer seasons following the ENSO developing and maturing months (e.g. Herceg-Bulić et al., 2017). It is also assumed that compositing of many ENSO events using long data cancel out the effects of other potential drivers on PDSI (except if any of them also coincides with ENSO) and therefore the PDSI composites obtained can only be connected to ENSO.

3. Results

To begin, we look into the PDSI during the instrumental period (Dai et al., 2004; Dai 2011). Shown in Fig. 1a–c are the PDSI composites for strong El Niños calculated by selecting the same events as by Brönnimann et al. (2007, B2007 hereafter); these do not include the extreme El Niño events and events following major volcanic eruptions. Note that our terminology in this paper

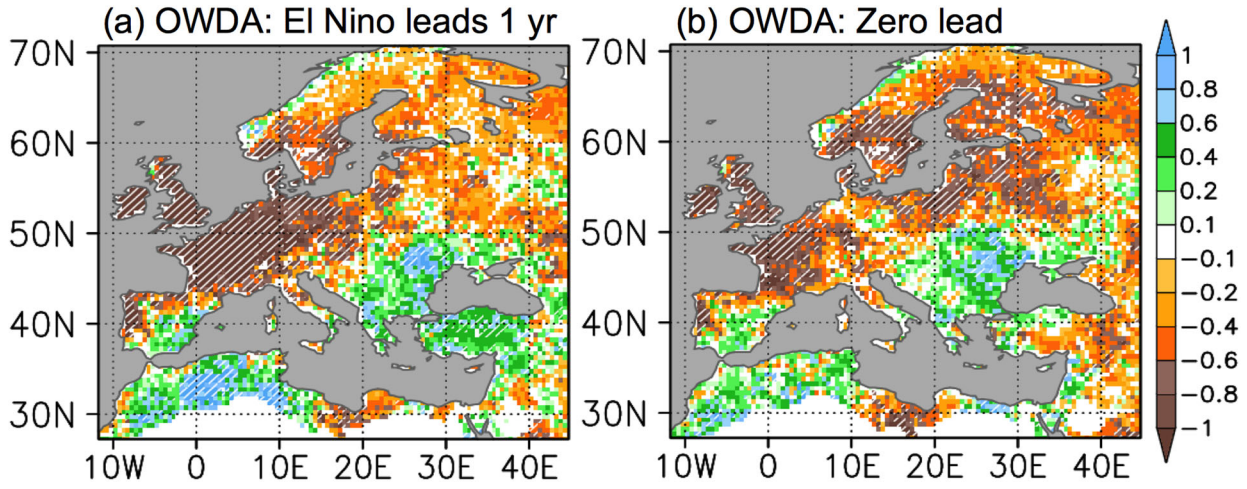

Fig. 2. Composites of PDSI for extreme El Nino years (at or above +2 S.D., 16 events) using OWDA and Li et al. (2011) ENSO index for 900–2002 C.E. Panel a: El Nino leads OWDA by 1 year; panel b: zero lead. See text on interpretation of lead or lag in this study. Grid points with at least 95% statistical significance are indicated with white hatching.

distinguishes between *strong* and *extreme* El Niños (explained further below). For this period, on average, a strong El Niño is accompanied by wet condition in western and southern Europe, and dry condition in northern Europe. This result confirms the finding of B2007, as well as that of Baek et al. (2017) who analysed both instrumental and tree-ring based PDSI for the years 1901–1978 (see their Fig. 4). Next, exactly the same analysis as above is repeated using the OWDA (Fig. 1d). Reassuringly, the OWDA and Dai et al.'s PDSI composites mostly agree with each other. Note that it may not be appropriate to compare PDSI with precipitation or temperature directly; however, warm and moist (cold and dry) air which are associated with winds from the Atlantic Ocean (Arctic) generally go together for locations in Europe especially during the cold seasons. This is largely due to the effect of NAO through which ENSO is affecting Europe climate (e.g. B2007, Brönnimann, 2007, King et al., 2018a, and references therein).

As mentioned above, in this paper we distinguish between *strong* or *extreme* ENSO. For Li et al.'s ENSO time series the extreme El Niños we selected have amplitudes at or larger than +2.0 standard deviation with average occurrence of once per 70 years; whereas strong El Niños are chosen to be between +1.0 and +2.0 standard deviation or an average occurrence of about once every 7–8 years. These thresholds are not based on any scientific principle, but were only determined by trial and error to obtain statistical significance or changes in the composites themselves. B2007 identifies three extreme El Niños in the twentieth century: 1973, 1983, 1998. The PDSI composites for these years are shown in Fig. 1e–g. Notably, the anomalies that are observed for strong El Niño above do not become even stronger for these extreme El Niños. Instead, dry condition is seen in large part of western Europe. Although the composite for OWDA under extreme El Niño (Fig. 1h) does not show the same intense and widespread dry condition seen for the Dai et al.'s PDSI (Fig. 1e–g), stronger wet or even just wet condition in western and southern Europe which is observed under strong El Niño is still not detected under extreme El Niño. Geng et al. (2017) reported the cooling observed in northern Europe during middle of January for the three most recent extreme (which they call "super") El Niños of 1982/83, 1997/98, 2015/16. Our further analysis on PDSI including the extreme El Niño of 2015/2016 shows that this latest event is consistent with Fig. 1h, where there is large area of drying in western, eastern and even southern Europe (figure not shown).

In order to improve on the robustness of the result for extreme El Niño shown in Fig. 1, we extend the composite analysis on OWDA further back in the last millennium using the Li et al. (2011) ENSO index. The result is shown in Fig. 2b. Extensive dry area in Europe is found under extreme El Niño. Because El Niño develops, matures and terminates over two different calendar years, there is a possible uncertainty on the timing recorded in the proxies. For this reason, we included the composite based on El Niño in the preceding year in Fig. 2a. The result of Fig. 2 indicates that it is indeed possible that extreme El Niño events are linked to dry conditions in large part of Europe, instead of north–south contrast of dry and wet conditions for strong El Niño events described earlier. We do not find any statistical significant European PDSI linked to extreme La Niña in OWDA. We note here that (perhaps disappointingly) OWDA only provides PDSI composites for strong ENSO

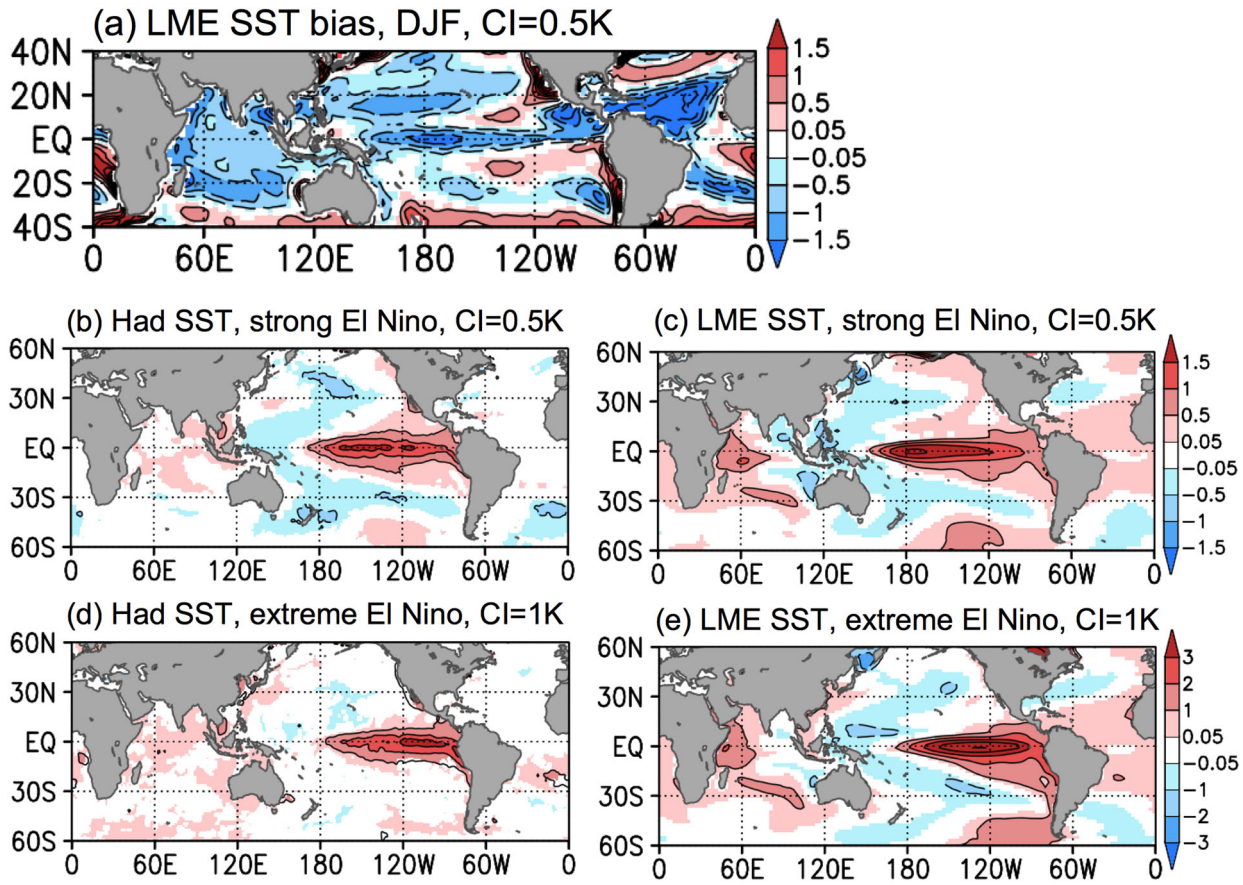

Fig. 3. Comparisons of CESM Last Millennium Experiment (LME) historical experiments (10 members) and Hadley Centre SST for DJF 1899–2003. Panel a is SST bias. Panels b, c are composites of SST anomalies for strong El Nino (+1 to +2 S.D. in Nino 3.4). Panels d, e are composites of SST anomalies for extreme El Nino (1972/73, 1982/83, 1997/98 for Had SST; at or above +2.5 S.D. in Nino 3.4 for LME). Colour shading also indicates 95% statistical significance. CI is contour interval.

in very limited areas (shown and discussed briefly at the end of this section).

Next, analysis of the CESM LME is presented. ENSO extratropical atmospheric teleconnection depends on Rossby wave-guiding due to background winds that can be determined by mean SST, as well as on the locations of ENSO SST anomalies in tropical Pacific. Figure 3 documents the mean SST bias and ENSO related SST anomalies in LME for the years 1899–2003. Panel a indicates that large parts of the tropical and subtropical SST in LME have a cold bias. Comparing panels b, d with c, e, respectively, also indicates that the LME has El Niño SST anomalies (by Niño3.4) in the tropical Pacific which are stronger than observation (by 0.5 K and 1.0 K at the maximum for strong and extreme El Niño, respectively), as well as with the maximum SST locations westward of those in observation. Ayarzaguena et al. (2018) show that for selected high-top CMIP5 models, the locations of the SST anomalies could be a more important factor in determining ENSO teleconnection to the Northern Hemisphere than the wave-guiding effect. We have examined the potential effects due to different ENSO types (see below) in LME, but our analyses are for only one model. Considering that the variability of ENSO-related SST anomalies is large in models (Cai et al., 2018), the range of PDSI composites for ENSO across different models is important and would require further studies.

The left column in Fig. 4 shows the composites for the strong El Niño, and right column the extreme El Niño. We believe these model results are robust as large samples are selected from many simulated years. Subsampling the years or members (i.e. selections of years or members in LME to create smaller sample sizes than the whole LME, and repeating the composite calculations) do not produce any important difference, indicating also that the internal variability has been removed adequately in the ENSO composites presented. The result on the right column is achieved by selecting extreme El Niños that happen once in about a century, which turns out to be Niño3.4 at or larger than +2.5 standard deviation. Noteworthy is the

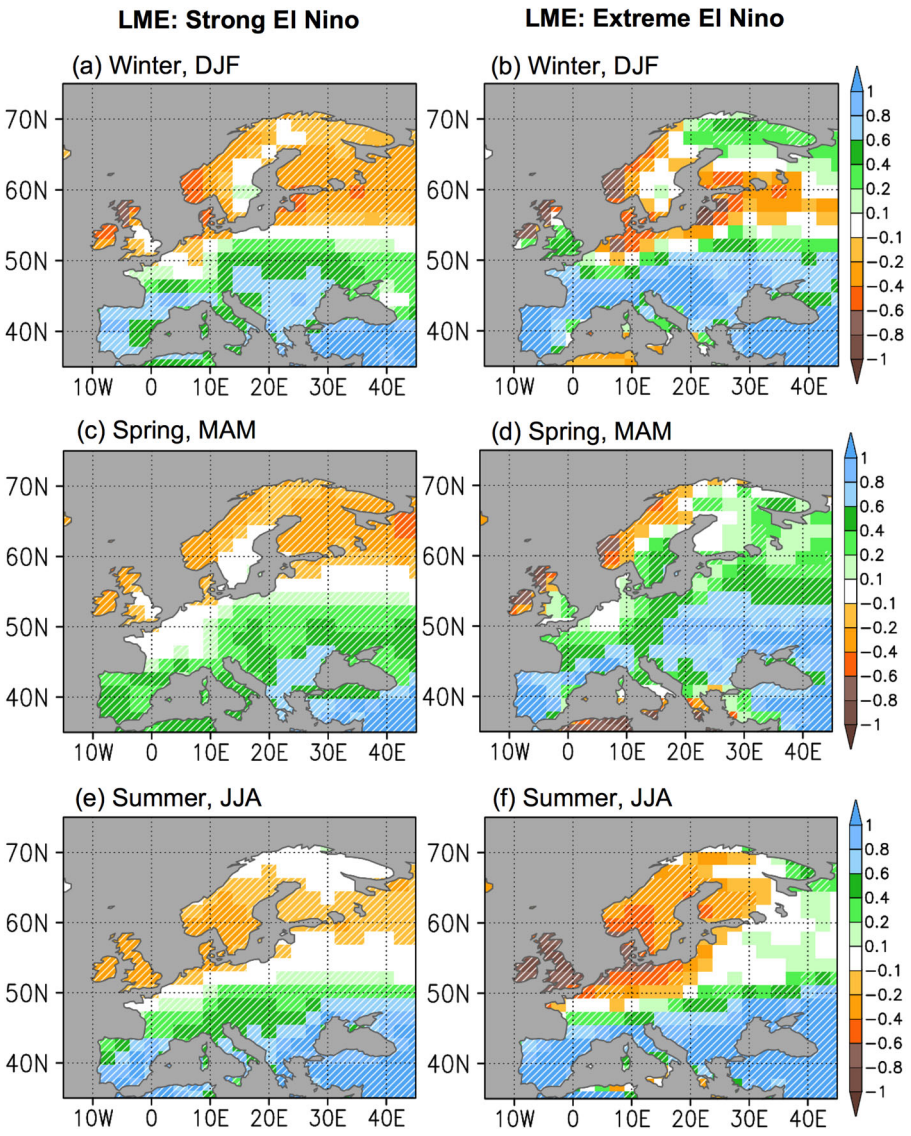

Fig. 4. Composites of PDSI in the seasons indicated for strong El Nino (left column; +1 to +2 S.D. in Nino3.4, 984 events) and for extreme El Nino years (right column; at or above +2.5 S.D. in Nino3.4, 121 events). These use a total of 11,560 years in total from CESM Last Millennium Experiment historical experiments (10 members). Grid points with at least 95% statistical significance are indicated with white hatching.

agreement in general features of the left panels in Fig. 4 with the top four panels in Fig. 1. This agreement also signifies the ability of the model to simulate PDSI correctly, although it is obvious that the model result is smoother compared to observational based PDSI, and depict anomalies with a clearer north–south structure. Stevenson et al. (2018) presented a similar analysis (regression instead of composite, see their Fig.1) in LME; their result also indicates generally wet (dry) condition in southern to southwestern Europe during El Niño (La Niña)

The PDSI associated with extreme El Niños in LME exhibits some degree of linearity to that for strong El Niños, and does not confirm the drying seen in western and central Europe for Dai et al.'s PDSI and OWDA under extreme El Niño. The summer season is more conducive for plant growth affecting tree-ring based OWDA, so the result for this season might be more relevant for the present comparison. Figure 4f indeed shows a stronger drying from the north extending to western Europe. The drying region however occurs in smaller area compared to those seen in lower four panels of Fig. 1 and in Fig. 2. The result from the model data gives further support to the current and previous findings on impact of *strong* El Niño, but the drying impact seen under *extreme* El Niños cannot be confirmed with CESM-LME.

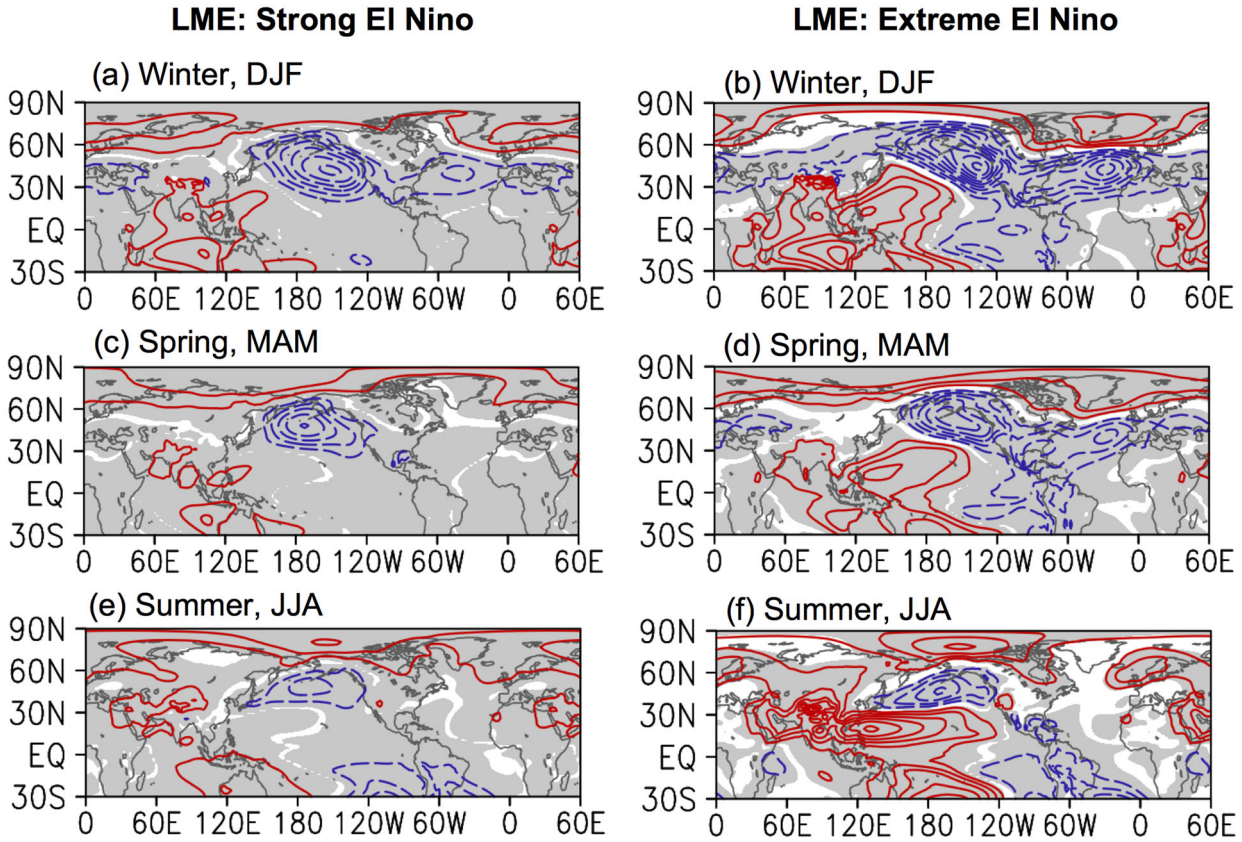

Fig. 5. Composites of sea-level pressure for strong El Ninos (left column; +1 to +2 S.D. in Nino3.4, 984 events) and for extreme El Nino years (right column; at or above +2.5 S.D. in Nino3.4, 121 events) and the seasons indicated (i.e. same as Fig. 4 except for SLP). These use a total 11,560 years of CESM Last Millennium Experiment historical experiments (10 members). Contour intervals = 1 hPa (top and middle rows), 0.5 hPa (bottom row). Grey shading indicates at least 95% statistical significance.

The atmospheric circulation and climate impacts of ENSO diversity have been reported previously (e.g. Ashok et al., 2007; King et al., 2018b and references therein). Here, additional checks using ENSO Modoki (as defined by Ashok et al., 2007), Niño3 and Niño4 indices for the LME and Dai et al's PDSI data have been performed. However, we do not find a substantial difference to the top panels of Fig. 1 and to Fig. 4. And in the case for the extreme of these indices, a resemblance to bottom panels of Fig. 1 and to Fig. 2 is not found. In particular, the negative PDSI anomaly for extreme El Niños that extends south of 50°N in these two figures are not seen in PDSI composites calculated using the additional indices representing different ENSO types. Therefore, it is believed that PDSI in Europe in the LME is not sensitive to different ENSO types.

In Fig. 5, the corresponding sea-level pressure (SLP) composites from the LME are shown. These provide some insight into the atmospheric circulation anomalies related to El Niño. There is no important qualitative difference in terms of the large-scale features between the strong and extreme El Niños simulated in LME; the features obtained are very typical for El Niño. There is a dipolar structure between western and eastern tropical Pacific (Southern Oscillation) and a strengthening of Aleutian Low in North Pacific; as well as a pattern that projects on the negative North Atlantic Oscillation (NAO). As mentioned in Section 2, the SST anomalies associated with ENSO have more extensive ocean areas globally in the LME (see Yu et al., 2018 and Fig. 3). Despite this, it is found that amplitudes of SLP anomalies associated with El Niño in DJF for LME (Fig. 5a) is also in agreement with observational data (see e.g. Fig. 10 in Deser et al., 2017). The simulated amplitudes of SLP composites for extreme El Niño are larger although the circulation anomalies in the NAE region are not fundamentally different, this likely explains the qualitative similarity for the PDSI composites in Fig. 4. As described above for Fig. 4, the north–south dipolar anomalies in PDSI are obtained for both strong and extreme El Niños in LME, and in a particular the negative PDSI anomalies that extend south of 50°N seen in Figs. 1 and 2 are not detected in LME.

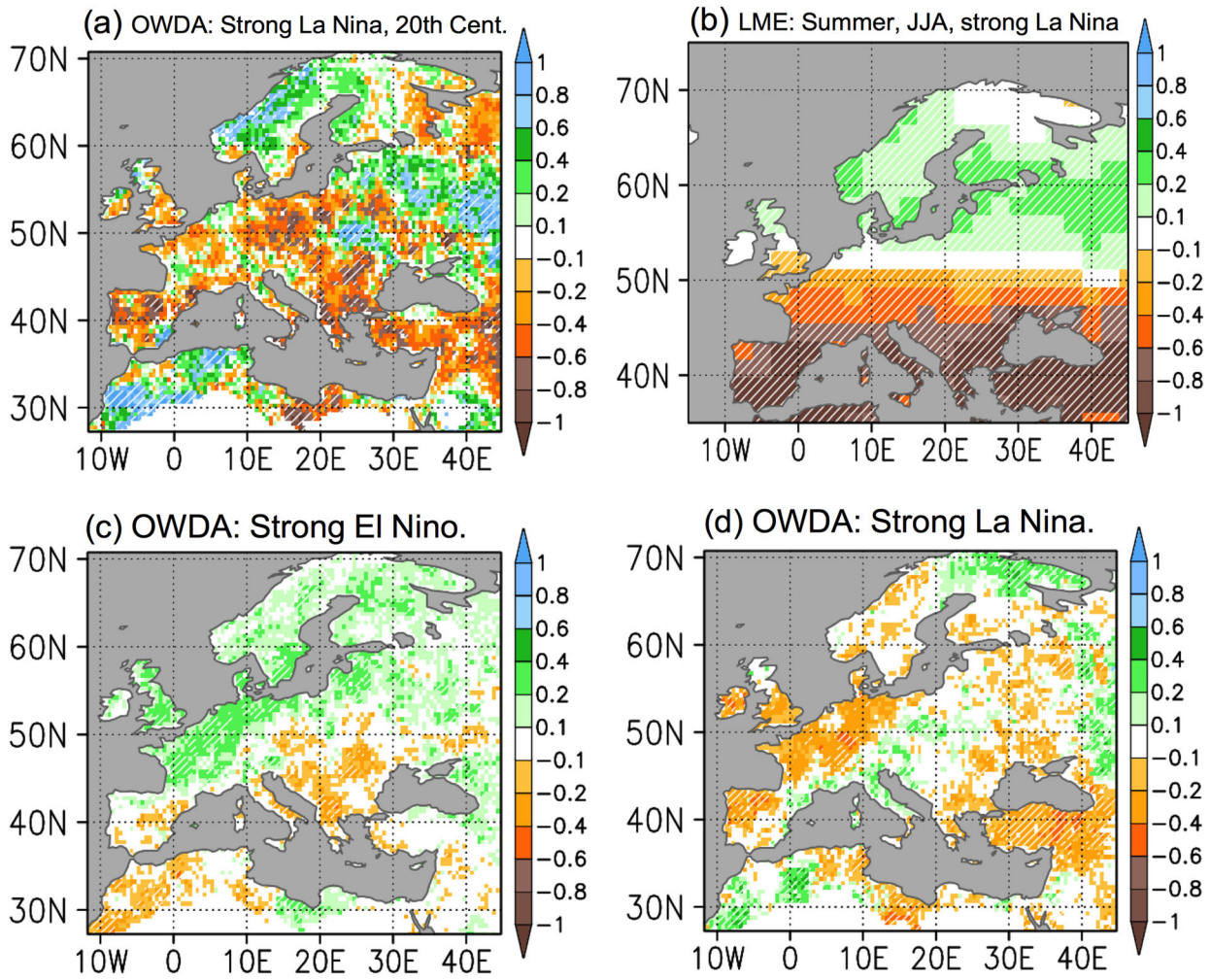

Fig. 6. Panel a is OWDA's PDSI composite for selected strong La Nina events same as Brönnimann et al. (2007) for the instrumental period and excluding events following volcanic eruptions. Panel b is composite of LME's PDSI for strong La Ninas (−1 to −2 S.D. in Nino3.4, 1089 events); these use a total 11,560 years of CESM Last Millennium Experiment historical experiments (10 members). Panels c, d are OWDA's PDSI composites for strong El Nino and La Nina events, respectively (between 1 and 2 S.D.). Grid points with at least 95% statistical significance are indicated with white colour hatching.

For completeness, four more composites are shown in Fig. 6. In panel a (correspond to Fig. 1d for El Niño), PDSI composite for La Niña events in the instrumental period as selected by Brönnimann (2007) is shown. Broadly speaking, the reverse of Fig. 1d is obtained, but region with statistical significance is very limited (also see Fig. 4 of Baek et al., 2017). In Fig. 6b, the strong La Niña composite for LME is almost the exact opposite of its El Niño counterpart in Fig. 4e. Again, the agreement of model and observational based PDSI in the general features indicates the model's ability in simulating PDSI correctly. The strong El Niño and La Niña composites for OWDA are shown in Fig. 6c and d, respectively. They are mostly symmetric of each other, but as mentioned before have very limited area of statistical significance. In any case, Fig. 6c does provide a further indication that strong El Niño's PDSI composite is not the same as the one for extreme El Niño (Fig. 2). Additionally, we have also examined the effects of moderate ENSO on PDSI in Dai et al.'s data and in LME. The results are qualitatively similar to strong ENSO, but with more limited area of statistical significance and the stronger anomalies are concentrated in southern Europe (not shown).

4. Concluding remarks

In this short paper, we report the possible impacts of ENSO on PDSI in Europe. This is not a new topic in itself. But here, we are interested in these relationships mainly in the relative new data of OWDA and CESM Last Millennium Ensemble, and how they compare with

previous findings. For OWDA in the last millennium, we find that only the most *extreme* El Niño events provide statistical significant PDSI anomaly (composite) in more extended area. This PDSI composite for *extreme* El Niño shows overall dry conditions in western, central, and northern Europe (Fig. 2b) which is different from the north–south pattern of respectively dry and wet conditions for *strong* El Niño reported by previous studies. The most recent *extreme* El Niños of 1972/1973, 1982/83, 1997/98, 2015/16 also produce a dry condition seen in western to central Europe. The north–south pattern, however, is indeed confirmed for OWDA in the instrumental period (Fig. 1d), Dai et al.'s PDSI (Fig. 1c), as well as the CESM-LME (Fig. 4e) for *strong* El Niño events. The 10-member LME data used is a particularly large sample. Subsampling of different members or different climate periods/epochs during the last millennium that can have different external climate forcings do not produce any result that is substantially different from those presented in Fig. 4. We found that CESM-LME over all years simulate the PDSI anomalies related to strong ENSO that are similar to the same anomalies obtained from Dai et al.'s PDSI and OWDA in the instrumental period (compare left column of Fig. 4 and top panels of Fig. 1; top row of Fig. 6). We believe this is a remarkable feat for the model considering the complex way PDSI is derived that takes into account the accumulative interaction, as well as the spatial variations, of the temperature and precipitation inputs.

There are two main issues that require further clarification or confirmation in future studies. Firstly, a dry western and northern Europe (Fig. 2) is associated with extreme El Niño in the OWDA data for the last millennium. This is also the case for both OWDA and Dai et al.'s PDSI during the instrumental period (Fig. 1e–h), but *not* confirmed with the CESM-LME. As far as we are aware, this impact of extreme El Niño in western to central Europe is not known (or at least not widely known). Confirming or refuting it will be an important step in understanding, predicting, and preparing for the climate impact in Europe. Implicit in this first issue is also the uncertainty or variability across models, in particular that related to the variability of ENSO SST anomalies across different models (Cai et al., 2018). Secondly, the reconstructed PDSI (OWDA in this case) does not show any statistical significant composite under strong ENSO in the last millennium (or any climate epoch within the last millennium we have examined, except during the instrumental period). This might be a disappointing result as the ENSO's hydroclimate impact that has a north–south structure in Europe is expected. There is a possibility that tree-ring based reconstructed PDSI cannot register this particular type of ENSO impact, or that only OWDA itself is deficient in this particular aspect. Furthermore, it is probably unlikely, but the OWDA's result may call into question the robustness of the "north–south" ENSO impact in Europe reported by a large body of previous studies. Clarifying both of these issues needs further analyses of other climate reconstruction and model data.

Acknowledgements

The OWDA (Cook et al., 2015) and CESM-LME (Otto-Bliesner et al., 2016) datasets have been essential for our study. Comments from Clio Michel and the reviewers on the manuscript have led to its improvements.

Disclosure statement

No potential conflict of interest was reported by the authors.

Funding

MPK and JS acknowledge the support of the Research Council of Norway under the ClimateXL project [No. 243953]. The data storage and analyses performed have used resources provided by UNINETT Sigma2 in Norway under project number NS9001K.

References

Ashok, K., Behera, S. K., Rao, S. A., Weng, H. and Yamagata, T. 2007. El Nino Modoki and its possible teleconnection. *J. Geophys. Res.* **112**, C11007:1–27. doi:10.1029/2006JC003798.

Ayarzaguena, B., Ineson, S., Dunstone, N. J., Baldwin, M. P. and Scaife, A. A. 2018. Intraseasonal effects of El Niño-Southern Oscillation on North Atlantic Climate. *J. Clim.* **31**, 8861–8873. doi:10.1175/JCLI-D-18-0097.1.

Baek, S. H., Smerdon, J. E., Coats, S., Williams, A. P., Cook, B. I. and co-authors. 2017. Precipitation, temperature, and teleconnection signals across the combined North American, monsoon Asia, and Old World Drought Atlases. *J. Clim.* **30**, 7141–7155. doi:10.1175/JCLI-D-16-0766.1.

Brönnimann, S. 2007. Impact of El Niño-Southern Oscillation on European climate. *Rev. Geophys.* **45**.

Brönnimann, S., Xoplaki, E., Casty, C., Pauling, A. and Luterbacher, J. 2007. ENSO influence on Europe during the last centuries. *Clim. Dyn.* **28**, 181–197. doi:10.1007/s00382-006-0175-z.

Cai, W., Borlace, S., Lengaigne, M., van Rensch, P., Collins, M. and co-authors. 2014. Increasing frequency of extreme El Niño events due to greenhouse warming. *Nat. Clim. Change* **4**, 111–116. doi:10.1038/nclimate2100.

Cai, W., Wang, G., Dewitte, B., Wu, L., Santoso, A. and co-authors. 2018. Increased variability of eastern Pacific El Niño

under greenhouse warming. *Nature* **564**, 201–206. doi:10.1038/s41586-018-0776-9.

Cai, W., Wang, G., Santoso, A., McPhaden, M. J., Wu, L. and co-authors. 2015. Increased frequency of extreme La Niña events under greenhouse warming. *Nat. Clim. Change* **5**, 132–137. doi:10.1038/nclimate2492.

Cook, E. R., Seager, R., Kushnir, Y., Briffa, K. R., Büntgen, U. and co-authors. 2015. Old World megadroughts and pluvials during the Common Era. *Sci. Adv.* **1**, e1500561. doi:10.1126/sciadv.1500561.

Dai, A. 2011. Characteristics and trends in various forms of the Palmer Drought Severity Index (PDSI) during 1900–2008. *J. Geophys. Res.* **116**, D12115. doi:10.1029/2010JD015541.

Dai, A., Trenberth, K. E. and Qian, T. 2004. A global dataset of Palmer Drought Severity Index for 1870–2002: relationship with soil moisture and effects of surface warming. *J. Hydrometeorol.* **5**, 1117–1130. doi:10.1175/JHM-386.1.

Deser, C., Simpson, I., McKinnon, K. and Phillips, A. 2017. The Northern Hemisphere extratropical atmospheric circulation response to ENSO: how well do we know it and how do we evaluate models accordingly? *J. Clim.* **30**, 5059–5082. doi:10.1175/JCLI-D-16-0844.1.

Geng, X., Zhang, W., Stuecker, M. F. and Jin, F.-F. 2017. Strong sub-seasonal wintertime cooling over East Asia and Northern Europe associated with super El Niño events. *Sci. Rep.* **7**, 3770. doi:10.1038/s41598-017-03977-2.

Herceg-Bulić, I., Mezzina, B., Kucharski, F., Ruggieri, P. and King, M. P. 2017. Wintertime ENSO influence on late spring European climate: the stratospheric response and the role of North Atlantic SST. *Int. J. Climatol.* **37**, 87–108. doi:10.1002/joc.4980.

Jacobi, J., Perrone, D., Duncan, L. L. and Hornberger, G. 2013. A tool for calculating the Palmer drought indices. *Water Resour. Res.* **49**, 6086–6089. doi:10.1002/wrcr.20342.

King, M. P., Herceg-Bulić, I., Bladé, I., García-Serrano, J., Keenlyside, N. and co-authors. 2018a. Importance of late fall ENSO teleconnection in the Euro-Atlantic sector. *Bull. Am. Meteorol. Soc.* **99**, 1337–1343. doi:10.1175/BAMS-D-17-0020.1.

King, M. P., Herceg-Bulić, I., Kucharski, F. and Keenlyside, N. 2018b. Interannual tropical Pacific sea surface temperature anomalies teleconnection to Northern Hemisphere atmosphere in November. *Clim. Dyn.* **50**, 1881–1899. doi:10.1007/s00382-017-3727-5.

Li, J., Xie, S. P., Cook, E. R., Huang, G., D'Arrigo, R., Liu, F., Ma, J., Zheng, X. T. 2011. Interdecadal modulation of El Niño amplitude during the past millennium. *Nat. Clim. Change*. **1**(2), 114–118. doi:10.1038/nclimate1086.

Otto-Bliesner, B., Brady, E., Fasullo, J., Jahn, A., Landrum, L. and co-authors. 2016. Climate variability and change since 850 C.E.: an ensemble approach with the Community Earth System Model (CESM). *Bull. Amer. Meteorol. Soc.* **97**, 735–754. doi:10.1175/BAMS-D-14-00233.1.

Raible, C. C., Bärenbold, O. and Gómez-Navarro, J. J. 2017. Drought indices revisited – improving and testing of drought indices in a simulation of the last two millennia for Europe. *Tellus A* **69**, 1287492. doi:10.1080/16000870.2017.1296226.

Scaife, A. A., Arribas, A., Blockley, E., Brookshaw, A., Clark, R. T. and co-authors. 2014. Skillful long-range of European and North American winters. *Geophys. Res. Lett.* **41**, 2514–2519. doi:10.1002/2014GL059637.

Scaife, A. A., Comer, R., Dunstone, N., Fereday, D., Folland, C. and co-authors. 2017. Predictability of European winter 2015/2016. *Atmos. Sci. Lett.* **18**, 38–44. doi:10.1002/asl.721.

Stevenson, S., Overpeck, J. T., Fasullo, J., Coats, S., Parsons, L. and co-authors. 2018. Climate variability, volcanic forcing, and last millennium hydroclimate extremes. *J. Clim.* **31**, 4309–4327. doi:10.1175/JCLI-D-17-0407.1.

Thornthwaite, C. W. 1948. An approach toward a rational classification of climate. *Geogr. Rev.* **38**, 55–94. doi:10.2307/210739.

van Oldenborgh, G. J. and Burgers, G. 2005. Searching for decadal variations in ENSO precipitation teleconnections. *Geophys. Res. Lett.* **32**, L15701:1–5. doi:10.1029/2005GL023110.

Wells, N., Goddard, S. and Hayes, M. J. 2004. A self-calibrating Palmer Drought Severity Index. *J. Clim.* **17**, 2335–2351. doi:10.1175/1520-0442(2004)017<2335:ASPDSI>2.0.CO;2.

Yu, E., King, M. P., Sobolowski, S., Otterå, O. H. and Gao, Y. Q. 2018. Asian droughts in the last millennium: a search for robust impacts of Pacific Ocean surface temperature variabilities. *Clim. Dyn.* 50, 4671–4689. doi:10.1007/s00382-017-3897-1.